Author(s): Tuovinen, Toni & Hinkkanen, Marko & Luomi, Jorma

Title: Modeling of Saturation Due to Main and Leakage Flux Interaction in Induction Machines

Year: 2010

Version: Post print

Please cite the original version:

Tuovinen, Toni & Hinkkanen, Marko & Luomi, Jorma. 2010. Modeling of Saturation Due to Main and Leakage Flux Interaction in Induction Machines. IEEE Transactions on Industry Applications. Volume 46, Issue 3. 937-945. ISSN 0093-9994 (printed). DOI: 10.1109/tia.2010.2045210.

Modeling of Saturation Due to Main and Leakage Flux Interaction in Induction Machines

Toni Tuovinen, Marko Hinkkanen, and Jorma Luomi
Department of Electrical Engineering
Helsinki University of Technology
P.O. Box 3000, FI-02015 TKK, Finland

***Abstract*—Saturation due to the main flux and rotor leakage flux interaction appears in induction machines, especially if the rotor slots are skewed or closed. Conventional saturation models used in connection with dynamic equivalent-circuit models do not take this phenomenon into account. In this paper, explicit functions for modeling this mutual saturation are proposed. These functions are physically reasonable, they are easy to fit, and the number of their parameters is small. The proposed functions can be used in real-time applications and in computer simulations if high accuracy and physical consistency are preferable. The model fits well to the data obtained from finite element analysis or experimental data of a 2.2-kW motor. The model predicts the stator current with good accuracy both in steady state and in transients.**

***Index Terms*—Induction motors, motor models, mutual saturation, closed slots, rotor skew.**

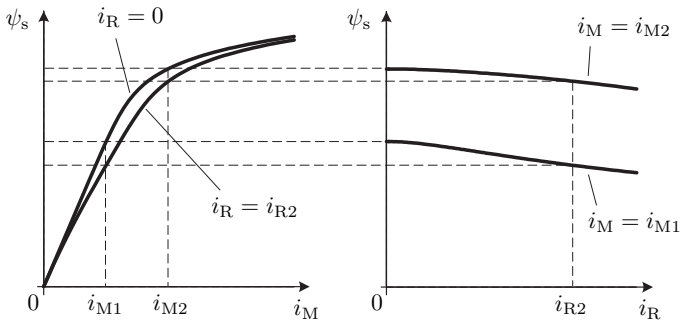

Fig. 1. Typical saturation characteristics of main flux $\psi_\mathrm{s}(i_\mathrm{M}, i_\mathrm{R})$. On the left-hand side, ψ_s is shown as a function of magnetizing current i_M for two different values of rotor current ($i_\mathrm{R}=0$ corresponding to no-load operation and i_R2 corresponding to constant rotor current). On the right-hand side, ψ_s is shown as a function of i_R for two values of i_M.

I. Introduction

Induction machines are usually magnetically saturated in the rated operating point. The main flux saturates strongly as a function of the magnetizing current. Furthermore, it has been observed that the main flux may depend significantly on the load (or the rotor current) due to the interaction between the main flux and the rotor leakage flux [1], [2]. This mutual saturation effect originates mainly from skewed and closed rotor slots [3], which are used in the majority of small machines. A typical main-flux saturation characteristics is sketched in Fig. 1; to model the inductance corresponding to the figure, a function of two variables is needed.

If the geometry of the machine and the material properties are known, magnetic saturation can be modeled with good accuracy using finite-element analysis (FEA). However, FEA is computationally too demanding for many applications, including real-time flux estimation in controlled drives, design of control algorithms, and simulations of transient phenomena. Instead, models based on lumped parameters, such as the equivalent circuit in Fig. 2, are commonly used.

In equivalent-circuit models, the magnetizing inductance is usually assumed to saturate only as a function of the magnetizing current or main flux [4], [5], [6]. The effects of the main flux saturation have been analyzed in [7], [8]. The leakage inductances have been modeled as functions of their own currents [4], [9]. For the magnetizing curve, explicit functions have been used, e.g. polynomials [10], [6], power functions [11], [4], and rational power functions [12]. In these previous models, the mutual saturation effect is omitted. The small-signal model proposed in [13] takes the mutual saturation effect into account, but no explicit functions are given for saturation characteristics.

The accuracy of the inductance model is important in various applications. If stator resistance adaptation is applied, the low-speed stability of speed-sensorless drives depends significantly on the inductance estimates [14]. In induction machines fed by frequency converters, the harmonic losses become dependent on the load current because of the mutual saturation [15]. The effects of magnetic saturation during transients can be more accurately analyzed by means of computer simulations if the mutual saturation effect is included in the dynamic model. For example, the effects of saturation induced saliencies are important when signal injection methods are used.

The inductance values of a machine cannot be measured directly. Usually, only the stator current, the stator voltage and the rotor speed are measured. If the magnetic saturation is modeled using functions, it is possible to obtain the function parameters by exploiting experimental data from several operating points [16].

In this paper, explicit functions are proposed for the saturation characteristics—including the mutual saturation. The inductances become functions of two variables (fluxes or currents). The proposed functions are physically reasonable, they are easy to fit, and the number of parameters is comparatively small. The proposed functions can be used in computer simulations where high accuracy and physical consistency are preferable. As an example, the inductance data of a 2.2-kW induction motor (obtained from FEA) are fitted to the

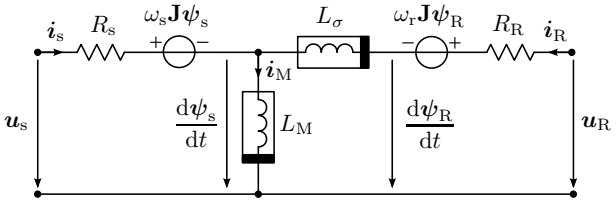

Fig. 2. Dynamic Γ model in coordinates rotating at angular speed ω_s, the angular slip frequency being ω_r.

proposed model, and a method to obtain the model parameters from laboratory measurements is demonstrated. A comparison between simulated and experimental stator currents is also given for a transient phenomenon.

II. Machine Model

As stated in [17], the T-equivalent dynamic model is more complex than necessary in the case of linear magnetics, and it is inadequate for use when the machine is saturated. Saturation effects appearing in machines equipped with closed or skewed rotor slots can be conveniently included in the Γ-equivalent model shown in Fig. 2, where the total leakage inductance is placed on the rotor side.

Real-valued space vectors will be used. They are denoted by boldface lowercase letters; for example, the stator current vector is $\boldsymbol{i}_s = [i_{sd}, i_{sq}]^T$ and its magnitude is

$$i_s = \sqrt{i_{sd}^2 + i_{sq}^2} \tag{1}$$

The orthogonal rotation matrix is

$$\mathbf{J} = \begin{bmatrix} 0 & -1 \\ 1 & 0 \end{bmatrix} \tag{2}$$

Since the saturation is to be modeled, it is convenient to choose the stator flux vector $\boldsymbol{\psi}_s$ and the rotor flux vector $\boldsymbol{\psi}_R$ as state variables, in order to avoid the differentiation of saturable inductances. In a synchronous coordinate system rotating at angular speed ω_s, the voltage equations of the induction machine are

$$\frac{d\boldsymbol{\psi}_s}{dt} = \boldsymbol{u}_s - R_s \boldsymbol{i}_s - \omega_s \mathbf{J}\boldsymbol{\psi}_s \tag{3a}$$

$$\frac{d\boldsymbol{\psi}_R}{dt} = \boldsymbol{u}_R - R_R \boldsymbol{i}_R - \omega_r \mathbf{J}\boldsymbol{\psi}_R \tag{3b}$$

where $\boldsymbol{u}_s$ is the stator voltage vector, R_s the stator resistance, $\boldsymbol{u}_R$ the rotor voltage vector, R_R the rotor resistance, and $\boldsymbol{i}_R$ the rotor current vector. The angular slip frequency is $\omega_r = \omega_s - \omega_m$, the electrical angular speed of the rotor being ω_m. The stator and rotor current vectors are

$$\boldsymbol{i}_s = \boldsymbol{\psi}_s / L_M - \boldsymbol{i}_R \tag{4a}$$

$$\boldsymbol{i}_R = (\boldsymbol{\psi}_R - \boldsymbol{\psi}_s) / L_\sigma \tag{4b}$$

respectively, where L_M is the magnetizing inductance and L_σ is the total leakage inductance. The leakage flux can be expresses as $\boldsymbol{\psi}_\sigma = L_\sigma \boldsymbol{i}_R$ and the main flux as $\boldsymbol{\psi}_s = L_M \boldsymbol{i}_M$, where $\boldsymbol{i}_M = \boldsymbol{i}_s + \boldsymbol{i}_R$ is the magnetizing current.

It is worth noticing that the flux vectors are assumed to be parallel with the corresponding current vectors in accordance with Fig. 2, while the scalar-valued inductances may be functions of the currents or fluxes. Inductances are assumed to be lossless. Hence, the inductances should fulfill the reciprocity condition [18], [3]:

$$\frac{\partial \psi_s}{\partial i_R} = \frac{\partial \psi_\sigma}{\partial i_M} \tag{5}$$

If needed, the iron losses can be taken into account separately [17], [19], [20]. A short-circuited rotor winding will be considered in this paper, i.e. $\boldsymbol{u}_R = [0, 0]^T$.

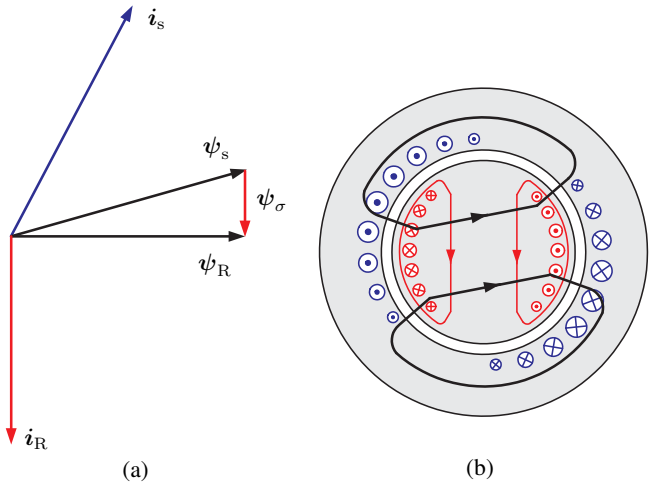

Fig. 3. (a) Space vector diagram and (b) magnetic flux paths: stator flux and rotor leakage flux.

III. Overview of Magnetic Saturation

If the stator slots are semi-closed (or open) as usual, the saturation of the stator leakage inductance is insignificant unless the current is very high. The stator leakage flux increases the load dependency of L_M only slightly.

A. Stator Flux and Leakage Flux

A vector diagram showing fluxes and currents of the Γ model is depicted in Fig. 3(a). The stator flux path and the leakage flux path are sketched in the motor cross-section in Fig. 3(b). The stator flux causes saturation principally in the teeth and yokes of the stator and the rotor.

In the case of closed rotor slots, the slot bridges provide a path for the rotor leakage flux. The leakage inductance L_σ saturates strongly as a function of the rotor current [21], [22]. The rotor flux is smaller than the stator flux due to the leakage flux since $\psi_R = \sqrt{\psi_s^2 - L_\sigma^2 i_R^2}$. Thus, increasing the rotor current should decrease the saturation in the rotor teeth and yoke. However, the leakage flux is nearly perpendicular to the stator flux, and it can be noticed in Fig. 3(b) that the saturation at the rotor surface and in the slot bridges caused by the rotor leakage flux appears in the stator flux path. Therefore, the magnetizing inductance L_M may saturate as a function of the rotor leakage flux (or the rotor current), particularly if the rotor slots are closed.

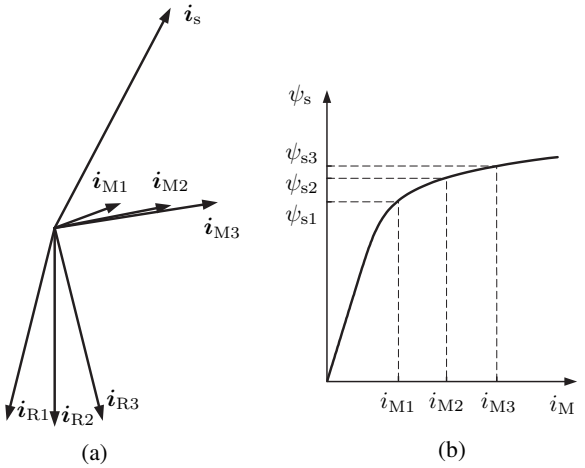

Fig. 4. Effect of skewed rotor when the motor consists of three slices with different rotor positions: (a) current space vectors and (b) saturation characteristics. Currents in the end slices are marked by subscripts 1 and 3 and currents in the middle slice by the subscript 2.

B. Rotor Skewing

Assuming linear magnetic properties, skewing the rotor slots reduces the magnetic coupling between the stator and rotor windings, and increases the leakage inductance [23]. The rotor skew also has an influence on the magnetic saturation, reducing the magnetizing inductance. A dominant effect is the change in the relative phase of the stator and rotor currents in the axial direction due to the skewed rotor bars, causing the saturation level of a loaded motor to vary in the axial direction. The decrease in flux at one end of the machine is not balanced by the increase of the flux at the other end of the machine [2].

A skewed motor can be considered to consist of an infinite number of elemental machines lying in radial planes and connected in series, with a gradual relative phase shift between the stator and rotor currents in the axial direction [24]. The motor is assumed to consist of three slices in Fig. 4(a), where the rotor current vectors are $\boldsymbol{i}_\mathrm{R1}$, $\boldsymbol{i}_\mathrm{R2}$, and $\boldsymbol{i}_\mathrm{R3}$ and the magnetizing current vectors are $\boldsymbol{i}_\mathrm{M1} = \boldsymbol{i}_\mathrm{s} + \boldsymbol{i}_\mathrm{R1}$, $\boldsymbol{i}_\mathrm{M2} = \boldsymbol{i}_\mathrm{s} + \boldsymbol{i}_\mathrm{R2}$, and $\boldsymbol{i}_\mathrm{M3} = \boldsymbol{i}_\mathrm{s} + \boldsymbol{i}_\mathrm{R3}$. The effect of magnetic saturation on the corresponding flux linkages ψ_s1, ψ_s2, and ψ_s3 is illustrated in Fig. 4(b). If a skewed motor is saturated, the magnetizing inductance

$$L_\mathrm{M} = \frac{\psi_\mathrm{s1} + \psi_\mathrm{s2} + \psi_\mathrm{s3}}{i_\mathrm{M1} + i_\mathrm{M2} + i_\mathrm{M3}} \tag{6}$$

becomes a function of the rotor current and decreases as the rotor current increases.

IV. Saturation Models

A. Conventional Functions

Conventionally, the saturable magnetizing inductance is modeled as

$$L_\mathrm{M}(\psi_\mathrm{s}) = \frac{\psi_\mathrm{s}}{i_\mathrm{M}(\psi_\mathrm{s})} \quad \text{or} \quad L_\mathrm{M}(i_\mathrm{M}) = \frac{\psi_\mathrm{s}(i_\mathrm{M})}{i_\mathrm{M}} \tag{7}$$

The first form is often preferred since $i_\mathrm{M}(\psi_\mathrm{s})$ can be modeled using polynomials or power functions. For example, the power function [11], [4]

$$i_\mathrm{M}(\psi_\mathrm{s}) = \frac{\psi_\mathrm{s}}{L_\mathrm{Mu}}\left(1 + \alpha\psi_\mathrm{s}^a\right) \tag{8}$$

includes only three parameters ($\alpha \geq 0$, $a \geq 0$, and the unsaturated inductance $L_\mathrm{Mu} > 0$). The resulting inductance function is

$$L_\mathrm{M}(\psi_\mathrm{s}) = \frac{L_\mathrm{Mu}}{1 + \alpha\psi_\mathrm{s}^a} \tag{9}$$

If needed, functions corresponding to (8) could be used to model $i_\mathrm{R}(\psi_\sigma)$. This kind of saturation models always fulfill (5), but they cannot model the mutual saturation effect. Instead of the power function (8), a polynomial could be used [10], [6].

B. Proposed Power Function

In this paper, the mutual saturation effect is taken into account by modeling the magnetizing inductance L_M and the rotor leakage inductance L_σ as

$$L_\mathrm{M}(\psi_\mathrm{s}, \psi_\sigma) = \frac{\psi_\mathrm{s}}{i_\mathrm{M}(\psi_\mathrm{s}, \psi_\sigma)} \tag{10a}$$

$$L_\sigma(\psi_\mathrm{s}, \psi_\sigma) = \frac{\psi_\sigma}{i_\mathrm{R}(\psi_\mathrm{s}, \psi_\sigma)} \tag{10b}$$

The goal is to find physically reasonable functions $i_\mathrm{M}(\psi_\mathrm{s}, \psi_\sigma)$ and $i_\mathrm{R}(\psi_\mathrm{s}, \psi_\sigma)$ fulfilling (5) and having a small number of parameters. It is convenient to consider functions of the form [25]

$$i_\mathrm{M}(\psi_\mathrm{s}, \psi_\sigma) = i'_\mathrm{M}(\psi_\mathrm{s}) + \frac{\mathrm{d}f(\psi_\mathrm{s})}{\mathrm{d}\psi_\mathrm{s}} g(\psi_\sigma) \tag{11a}$$

$$i_\mathrm{R}(\psi_\mathrm{s}, \psi_\sigma) = i'_\mathrm{R}(\psi_\sigma) + f(\psi_\mathrm{s}) \frac{\mathrm{d}g(\psi_\sigma)}{\mathrm{d}\psi_\sigma} \tag{11b}$$

The function (8) is adopted for $i'_\mathrm{M}(\psi_\mathrm{s})$ and $i'_\mathrm{R}(\psi_\sigma)$. The mutual saturation effect is modeled with power functions: $f(\psi_\mathrm{s}) \propto \psi_\mathrm{s}^{c+2}$ and $g(\psi_\sigma) \propto \psi_\sigma^{d+2}$.

The resulting saturation characteristics are

$$i_\mathrm{M}(\psi_\mathrm{s}, \psi_\sigma) = \frac{\psi_\mathrm{s}}{L_\mathrm{Mu}}\left(1 + \alpha\psi_\mathrm{s}^a + \frac{\gamma L_\mathrm{Mu}}{d+2}\psi_\mathrm{s}^c\psi_\sigma^{d+2}\right) \tag{12a}$$

$$i_\mathrm{R}(\psi_\mathrm{s}, \psi_\sigma) = \frac{\psi_\sigma}{L_{\sigma\mathrm{u}}}\left(1 + \beta\psi_\sigma^b + \frac{\gamma L_{\sigma\mathrm{u}}}{c+2}\psi_\mathrm{s}^{c+2}\psi_\sigma^d\right) \tag{12b}$$

where $\{\alpha, \beta, \gamma\} \geq 0$ and $\{a, b, c, d\} \geq 0$. It can be easily shown that the condition (5) holds. Furthermore, any other functions could be used for $i'_\mathrm{M}(\psi_\mathrm{s})$ and $i'_\mathrm{R}(\psi_\sigma)$ without violating the reciprocity condition. The inductances corresponding to (12) are

$$L_\mathrm{M}(\psi_\mathrm{s}, \psi_\sigma) = \frac{L_\mathrm{Mu}}{1 + \alpha\psi_\mathrm{s}^a + \frac{\gamma L_\mathrm{Mu}}{d+2}\psi_\mathrm{s}^c\psi_\sigma^{d+2}} \tag{13a}$$

$$L_\sigma(\psi_\mathrm{s}, \psi_\sigma) = \frac{L_{\sigma\mathrm{u}}}{1 + \beta\psi_\sigma^b + \frac{\gamma L_{\sigma\mathrm{u}}}{c+2}\psi_\mathrm{s}^{c+2}\psi_\sigma^d} \tag{13b}$$

If no mutual saturation existed in the machine to be analyzed, parameter γ would be zero and the model would be identical to the model proposed in [11].

V. Parameter Identification

A. Direct Method

The currents and the fluxes of the machine can be computed using FEA at different operating points, and the corresponding magnetizing inductance L_{M} and leakage inductance L_σ can be evaluated directly from the results. The parameters of the proposed model are fitted by minimizing the cost function

$$J(L_{\mathrm{Mu}}, L_{\sigma\mathrm{u}}, \alpha, \beta, \gamma, a, b, c, d) = \sum_{n=1}^{N} \left(\hat{L}_{\mathrm{M},n} - L_{\mathrm{M},n}\right)^2 + \left(\hat{L}_{\sigma,n} - L_{\sigma,n}\right)^2 \quad (14)$$

where the inductance estimates $\hat{L}_{\mathrm{M}}$ and $\hat{L}_\sigma$ are calculated from the proposed functions (13) using the actual values of the fluxes ψ_{s} and ψ_σ in each operating point. The index n refers to an operating point and N is the total number of different operating points.

B. Indirect Method

The inductances of the induction machine cannot be measured directly. However, the parameters of the inductance functions (13) can be identified indirectly based on more easily measurable variables: the stator voltage $\boldsymbol{u}_{\mathrm{s}}$, the stator current $\boldsymbol{i}_{\mathrm{s}}$, and the angular speed ω_{m} of the rotor. The identification method is based on steady-state measurements.

1) No-Load Test: First, the stator resistance R_{s} is measured. Then, the machine is operated in steady state at no load at various voltage levels. At each operating point, the estimate $\hat{\boldsymbol{\psi}}_{\mathrm{s}}$ of the stator flux is determined based on the stator voltage equation (3a):

$$\hat{\boldsymbol{\psi}}_{\mathrm{s}} = -\mathbf{J}\left(\boldsymbol{u}_{\mathrm{s}} - R_{\mathrm{s}}\boldsymbol{i}_{\mathrm{s}}\right)/\omega_{\mathrm{s}} \quad (15)$$

Considering (13a) at no load, the stator current estimate can be expressed as

$$\hat{\boldsymbol{i}}_{\mathrm{s}} = \frac{\hat{\boldsymbol{\psi}}_{\mathrm{s}}}{L_{\mathrm{Mu}}}(1 + \alpha\hat{\psi}_{\mathrm{s}}^a) \quad (16)$$

at every operating point, since the rotor current is zero. The cost function to be minimized is

$$J(L_{\mathrm{Mu}}, \alpha, a) = \sum_{n=1}^{N} \left|\left|\hat{\boldsymbol{i}}_{\mathrm{s},n} - \boldsymbol{i}_{\mathrm{s},n}\right|\right|^2 \quad (17)$$

2) Load Test: The parameters L_{Mu}, α, and a are known after the no-load test. It was found that the exponents b, c, and d have a relatively small effect on the resulting saturation characteristics, but they make the fitting process more difficult. Therefore, parameter values $b = 1$, $c = 1$ and $d = 0$ were fixed. To determine the remaining parameters of the inductance model (13), the motor is operated at various voltage levels and at various non-zero slip frequencies.

The stator flux estimate $\hat{\boldsymbol{\psi}}_{\mathrm{s}}$ is evaluated independently of the inductance model (13) using the stator voltage equation (15). The rotor current estimate can be expressed as

$$\hat{\boldsymbol{i}}_{\mathrm{R}} = \frac{\hat{\boldsymbol{\psi}}_{\mathrm{s}}}{L_{\mathrm{Mu}}}\left(1 + \alpha\hat{\psi}_{\mathrm{s}}^a + \frac{\gamma L_{\mathrm{Mu}}}{2}\hat{\psi}_{\mathrm{s}}\hat{\psi}_\sigma^2\right) - \boldsymbol{i}_{\mathrm{s}} \quad (18)$$

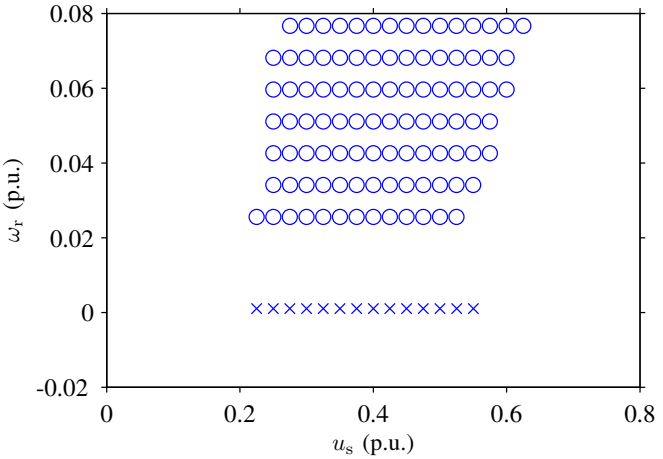

Fig. 5. Stator voltage magnitudes and angular slip frequencies used in parameter estimation from the FEA data. Circles denote the data used in load tests, crosses denote the no-load data. The stator frequency is 0.5 p.u.

in accordance with (12a). The leakage flux estimate can be solved from the rotor voltage equation (3b),

$$\hat{\boldsymbol{\psi}}_\sigma = -\frac{\hat{\boldsymbol{i}}_{\mathrm{R}}^{\mathrm{T}}\hat{\boldsymbol{\psi}}_{\mathrm{s}}}{\hat{\boldsymbol{i}}_{\mathrm{R}}^{\mathrm{T}}\hat{\boldsymbol{i}}_{\mathrm{R}}}\hat{\boldsymbol{i}}_{\mathrm{R}} \quad (19)$$

At each operating point, the leakage flux estimate $\hat{\boldsymbol{\psi}}_\sigma$ can be analytically solved from (18) and (19) for any given value of γ. Then, the estimated currents corresponding to (12) can be evaluated:

$$\hat{\boldsymbol{i}}_{\mathrm{M}} = \frac{\hat{\boldsymbol{\psi}}_{\mathrm{s}}}{L_{\mathrm{Mu}}}\left(1 + \alpha\hat{\psi}_{\mathrm{s}}^a + \frac{\gamma L_{\mathrm{Mu}}}{2}\hat{\psi}_{\mathrm{s}}\hat{\psi}_\sigma^2\right) \quad (20a)$$

$$\hat{\boldsymbol{i}}_{\mathrm{R}} = \frac{\hat{\boldsymbol{\psi}}_\sigma}{L_{\sigma\mathrm{u}}}\left(1 + \beta\hat{\psi}_\sigma + \frac{\gamma L_{\sigma\mathrm{u}}}{3}\hat{\psi}_{\mathrm{s}}^3\right) \quad (20b)$$

The values for $L_{\sigma\mathrm{u}}$, β, and γ are obtained by minimizing

$$J(L_{\sigma\mathrm{u}}, \beta, \gamma) = \sum_{n=1}^{N} \left|\left|\hat{\boldsymbol{i}}_{\mathrm{s},n} - \boldsymbol{i}_{\mathrm{s},n}\right|\right|^2 \quad (21)$$

where $\hat{\boldsymbol{i}}_{\mathrm{s}} = \hat{\boldsymbol{i}}_{\mathrm{M}} - \hat{\boldsymbol{i}}_{\mathrm{R}}$. It is worth noticing that there are alternative ways to indirectly identify the parameters of the inductance model; in the method described above, the values of the angular slip frequency ω_{r} are needed only if the values of the rotor resistance are of interest.

VI. Results

Saturation characteristics of a 2.2-kW squirrel-cage induction machine were studied by means of two-dimensional time-harmonic FEA [26], [27] and laboratory experiments. The machine is equipped with closed and skewed rotor slots, and its rating is: voltage 400 V; current 5 A; frequency 50 Hz; speed 1436 r/min; and torque 14.6 Nm. The base values are: angular frequency $2\pi 50$ rad/s; voltage $\sqrt{2/3}\cdot 400$ V; and current $\sqrt{2}\cdot 5$ A. The rotor skew was modeled using six motor slices in the FEA.

TABLE I
FITTED PER-UNIT PARAMETERS OBTAINED FROM FEA DATA AND EXPERIMENTAL DATA

	FEA Direct	FEA Indirect	Experimental
L_{Mu}	2.65	2.65	2.28
$L_{\sigma\mathrm{u}}$	1.48	0.441	0.216
α	0.406	0.429	0.383
β	10.5	3.86	0.511
γ	6.49	3.18	3.20
a	9.0	9.0	7.5
b	0.5	1.0	1.0
c	0.5	1.0	1.0
d	0.5	0.0	0.0

A. Finite Element Analysis

The operating points used in parameter estimation from the FEA data are presented in Fig. 5. The stator frequency ω_{s} was 0.5 p.u. in order to reach the stator flux value 1.1 p.u. within the rated voltage limit.

1) Direct Method: The parameters of the proposed model (13) were identified based on the inductance data obtained from FEA. The direct method presented in Section V-A was used. Since fractional exponents may be computationally inefficient, the exponents a, b, c, and d were rounded to the nearest half-integers (or integers) after the first fitting, and the other parameters were re-fitted. The cost function (14) was minimized using the Matlab function fminsearch. The fitted per-unit parameters are given in Table I.

The inductance data from FEA and the curves from the fitted functions are shown in Fig. 6. In Fig. 6(a), the magnetizing inductance L_{M} is shown as a function of ψ_{s} for three different values of ψ_σ. In Fig. 6(b), L_{M} is shown as a function of ψ_σ for three different values of ψ_{s}. Similar representation for the rotor leakage inductance L_σ is used in Figs. 6(c) and 6(d).

It can be seen that the proposed model for L_{M} fits very well to the FEA data. The mutual saturation appears to be very significant in the analyzed machine; in the case of no mutual saturation, the curves in Fig. 6(a) would overlap while the curves in Fig. 6(b) would be straight horizontal lines.

The differences in L_σ between the FEA data and the fitted curves at low values of ψ_σ are partly due to numerical problems in FEA; the rotor-side parameters cannot be determined reliably if the rotor current is close to zero. Furthermore, the peak in L_σ in the vicinity of $\psi_{\mathrm{s}} \approx 1.0$ p.u. is not consistent with the reciprocity condition; there should be similar peak in L_{M} as a function of ψ_σ. Obviously, any simple equivalent-circuit model cannot capture all the nonlinearities of the FEA solution.

2) Indirect Method: The indirect method presented in Section V-B is demonstrated by first applying it to the FEA data. The stator resistance was fixed to R_{s} = 0.0795 p.u. based on the FEA data. The cost function (21) was minimized using the Matlab function fminsearch. The fitted per-unit parameters are given in Table I.

It can be noticed that the parameter values, particularly $L_{\sigma\mathrm{u}}$, β and γ, differ from those obtained by using the direct method. The different value of exponent b has an effect on parameters $L_{\sigma\mathrm{u}}$ and β, whereas different values for c and d has an effect on parameter γ.

The inductance data from FEA and the curves from the fitted functions are shown in Fig. 7 in a fashion similar to Fig. 6. The differences between the curves obtained by using the direct method (Fig. 6) and indirect method (Fig. 7) are small.

B. Experiments

In the laboratory experiments, the 2.2-kW induction machine was fed by a frequency converter controlled by a dSPACE DS1103 PPC/DSP board. The dc-link voltage was measured, and a simple current feedforward compensation for dead times and power device voltage drops was applied [28]. All three phase currents were measured, and the components i_{sd} and i_{sq} of the stator current vector $\boldsymbol{i}_{\mathrm{s}}$ were calculated. The sampling was synchronized to the modulation, and both the switching frequency and the sampling frequency were 5 kHz.

1) Steady State: At each operating point, the stator frequency was $\omega_{\mathrm{s}} = 0.5$ p.u., while the magnitude of the stator voltage was varied. The stator frequency was chosen to be lower than the rated value, in order to reach the stator flux value 1.1 p.u. within the rated voltage limit. The slip frequency ω_{r} was adjusted using a servo motor.

The indirect method was used to identify the parameters of the inductance model based on experimental data. The stator resistance was fixed to R_{s} = 0.0628 p.u. obtained from a dc test. The operating points used in indirect parameter estimation from the experimental data are presented in Fig. 8.

The resulting inductance values are depicted in Fig. 9 in a fashion similar to Figs. 6 and 7, and the fitted per-unit parameters are given in Table I. Comparing Figs. 7(a,b) to Figs. 9(a,b), it can be noticed that the magnetizing inductance function fitted to the FEA data corresponds well to that fitted to the experimental data. Comparison of Figs. 7(c,d) and Figs. 9(c,d) reveals a difference in the case of the leakage inductance. This difference is related to the geometry and material properties models used in the FEA: the thickness of the rotor slot bridges is uncertain due to tolerances associated with the punching of the rotor sheets, and the degradation of magnetic properties of these very thin bridges is not modeled.

For comparison, the estimated and measured stator currents are depicted in Fig. 10. In Fig. 10(a), the magnitude of the stator current vector i_{s} is shown as a function of the magnitude of the stator voltage vector u_{s} for three different values of the angular slip frequency ω_{r}. In Fig. 10(b), i_{s} is shown as a function of ω_{r} for three different values of u_{s}. Similar representation for the displacement power factor $\cos\varphi$ is used in Figs. 10(c) and 10(d). The values of the stator current were obtained by inserting the stator voltage and the slip frequency into the motor model and finding the values for $\boldsymbol{\psi}_{\mathrm{s}}$ and $\boldsymbol{\psi}_\sigma$ that satisfied the voltage equations (3) in steady state. The model predicts the magnitude of the stator current and the displacement power factor with good accuracy.

In addition to the model parameters given in Table I, an estimate for the rotor resistance value was needed in order to estimate the stator current as a function of ω_{r}. After $\hat{\boldsymbol{\psi}}_\sigma$ and

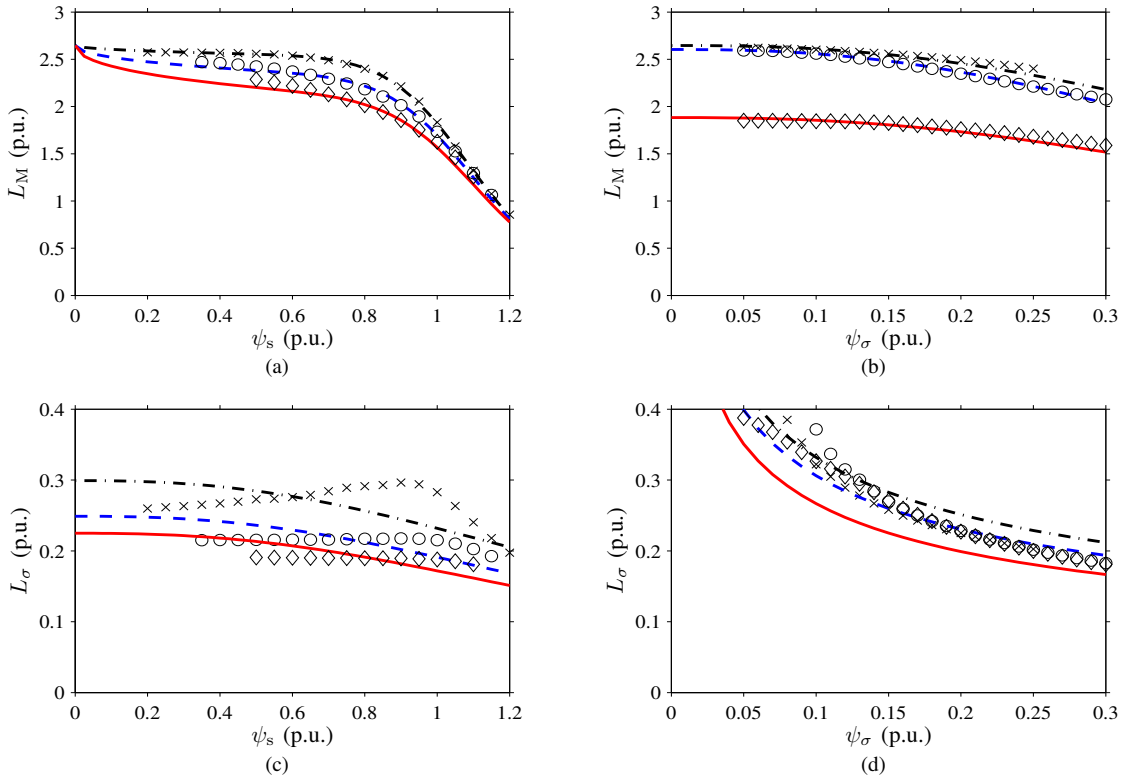

Fig. 6. Results of direct method applied to the inductance values obtained from the FEA data: (a) L_{M} as a function of ψ_{s} for three different values of ψ_{σ}, (b) L_{M} as a function of ψ_{σ} for three different values of ψ_{s}, (c) leakage inductance L_{σ} as a function of ψ_{s} for three different values of ψ_{σ}, (d) L_{σ} as a function of ψ_{σ} for three different values of ψ_{s}. In (a) and (c), the values of ψ_{σ} correspond to $i_{\mathrm{R}} \approx 0.5$ p.u. (dash-dotted line), $i_{\mathrm{R}} \approx 1.0$ p.u. (dashed line) and $i_{\mathrm{R}} \approx 2.0$ p.u. (solid line). In (b) and (d), the values of ψ_{s} are 0.4 p.u. (dash-dotted line), 0.7 p.u. (dashed line) and 1.0 p.u. (solid line).

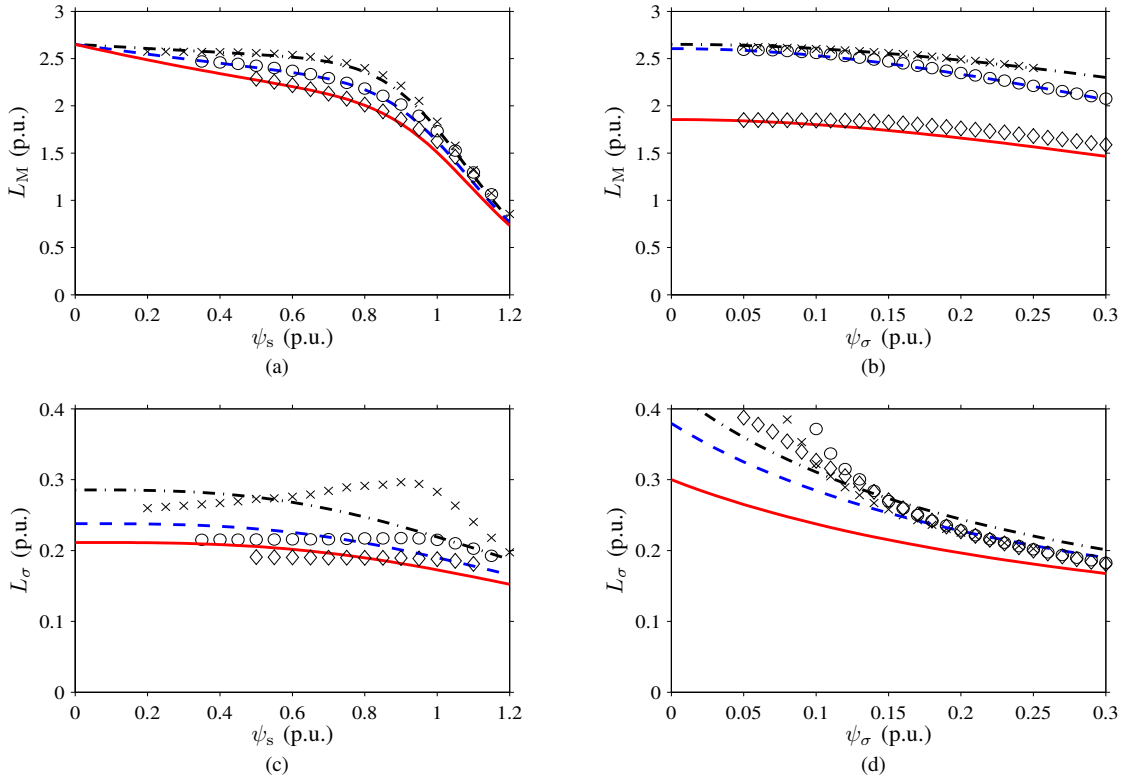

Fig. 7. Results of indirect method applied to the FEA data: (a) L_{M} as a function of ψ_{s} for three different values of ψ_{σ}, (b) L_{M} as a function of ψ_{σ} for three different values of ψ_{s}, (c) L_{σ} as a function of ψ_{s} for three different values of ψ_{σ}, (d) L_{σ} as a function of ψ_{σ} for three different values of ψ_{s}. In (a) and (c), the values of ψ_{σ} correspond to $i_{\mathrm{R}} \approx 0.5$ p.u. (dash-dotted line), $i_{\mathrm{R}} \approx 1.0$ p.u. (dashed line) and $i_{\mathrm{R}} \approx 2.0$ p.u. (solid line). In (b) and (d), the values of ψ_{s} are 0.4 p.u. (dash-dotted line), 0.7 p.u. (dashed line) and 1.0 p.u. (solid line).

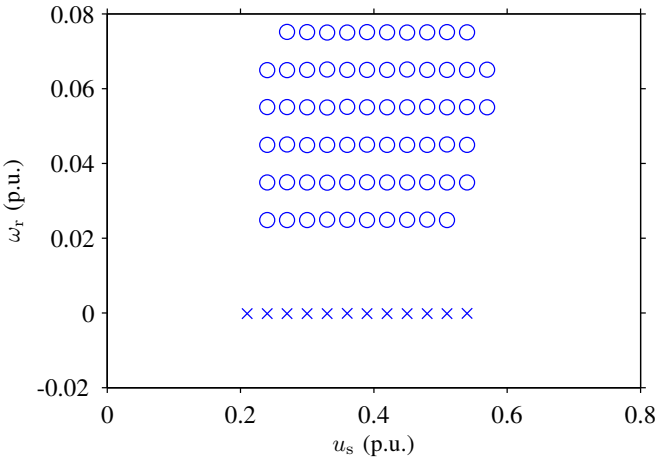

Fig. 8. Stator voltage magnitudes and angular slip frequencies used in indirect parameter estimation from the experimental data. Circles denote the data used in load tests, crosses denote the no-load data. The stator frequency is 0.5 p.u.

$\hat{\boldsymbol{i}}_\mathrm{R}$ were solved from (18) and (19) in every operation point used in the indirect parameter estimation, $\hat{R}_\mathrm{R}$ was solved from the rotor voltage equation (3b) in steady state. The mean value $\hat{R}_\mathrm{R} = 0.0416$ p.u. was used in the stator current estimation.

2) Transient State: The dynamic properties of the proposed model were studied in a transient test. The rotor was locked in order to avoid changes in the rotor speed. Initially, ω_s was 0.2 p.u. At t = 3.0 s, ω_s was reversed to -0.2 p.u. The magnitude of the stator voltage was 0.15 p.u. The parameters obtained from the experimental data using the indirect estimation method were used in the simulation model.

In addition to the model parameters given in Table I, an estimate for the rotor resistance value was needed for simulation purposes. The data obtained from a locked-rotor test was used. Using the estimation method described in Section VI-B1, the value $\hat{R}_\mathrm{R} = 0.0433$ p.u. was obtained.

The measured stator current and the simulated stator current are depicted in Fig. 11 as a function of time. The magnitude i_s of the stator current was evaluated according to (1). In Fig. 11(a), the simulation model includes the mutual saturation effect. In Fig. 11(b), the mutual saturation effect has been omitted. The behavior of i_s, particularly the first peak after t = 3.0 s, is predicted more accurately by the simulation model that includes the mutual saturation effect.

The particular transient test was chosen since it is easy to present without unduly extending the manuscript. In this test, the disturbances caused by speed oscillations are eliminated, and it shows that the model has influence on the large-signal behavior of the motor. The modeling improvements can be seen more clearly in parameter identification methods that are based on signal injection and in stator resistance adaptation. The authors plan to include these results in a future publication.

VII. Conclusions

Mutual saturation between the main flux and the rotor leakage flux appearing in induction machines can be modeled analytically. The proposed functions are physically reasonable, and the number of their parameters is small. The functions can be used in real-time applications and in computer simulations where high accuracy and physical consistency are preferable. The model fits well to the data obtained from finite element analysis and to the experimental data for a 2.2-kW induction motor with closed and skewed rotor slots. The model predicts the stator current with good accuracy both in steady state and in transient state.

Acknowledgment

This work was supported by the Finnish Funding Agency for Technology and Innovation, ABB Oy, Kone Oyj, and High Speed Tech Oy Ltd.

References

[1] A. Yahiaoui and F. Bouillault, "Saturation effect on the electromagnetic behaviour of an induction machine," *IEEE Trans. Magn.*, vol. 31, no. 3, pp. 2036–2039, May 1995.

[2] C. Gerada, K. J. Bradley, M. Sumner, and P. Sewell, "Evaluation and modelling of cross saturation due to leakage flux in vector controlled induction machines," *IEEE Trans. Ind. Appl*, vol. 43, no. 3, pp. 694–702, May/June 2007.

[3] M. Hinkkanen, A.-K. Repo, and J. Luomi, "Influence of magnetic saturation on induction motor model selection," in *Proc. ICEM'06*, Chania, Greece, Sept. 2006, CD-ROM.

[4] N. R. Klaes, "Parameter identification of an induction machine with regard to dependencies on saturation," *IEEE Trans. Ind. Appl.*, vol. 29, no. 6, pp. 1135–1140, Nov./Dec. 1993.

[5] E. Levi, "Main flux saturation modelling in double-cage and deep-bar induction machines," *IEEE Trans. Energy Convers.*, vol. 11, no. 2, pp. 305–311, June 1996.

[6] S. D. Sudhoff, D. C. Aliprantis, B. T. Kuhn, and P. L. Chapman, "Experimental characterization procedure for use with an advanced induction machine model," *IEEE Trans. Energy Convers.*, vol. 18, no. 1, pp. 48–56, Mar. 2003.

[7] K. P. Kovács, "On the theory of cylindrical rotor a.c. machines, including main flux saturation," *IEEE Trans. Power App. Syst.*, vol. PAS-103, no. 4, pp. 754–761, Apr. 1984.

[8] P. Vas, K. E. Hallenius, and J. E. Brown, "Cross-saturation in smooth-air-gap electrical machines," *IEEE Trans. Energy Convers.*, vol. 1, no. 1, pp. 103–112, Mar. 1986.

[9] R. C. Healey, S. Williamson, and A. C. Smith, "Improved cage rotor models for vector controlled induction motors," *IEEE Trans. Ind. Appl.*, vol. 31, no. 4, pp. 812–822, July/Aug. 1995.

[10] J. A. Melkebeek and J. L. Willems, "Reciprocity relations for the mutual inductances between orthogonal axis windings in saturated salient-pole machines," *IEEE Trans. Ind. Appl.*, vol. 26, no. 1, pp. 107–114, Jan./Feb. 1990.

[11] H. C. J. de Jong, "Saturation in electrical machines," in *Proc. ICEM'80*, vol. 3, Athens, Greece, Sept. 1980, pp. 1545–1552.

[12] C. R. Sullivan and S. R. Sanders, "Models for induction machines with magnetic saturation of the main flux path," *IEEE Trans. Ind. Appl*, vol. 31, no. 4, pp. 907–917, July/Aug. 1995.

[13] M. Hinkkanen, A.-K. Repo, M. Cederholm, and J. Luomi, "Small-signal modelling of saturated induction machines with closed or skewed rotor slots," in *Conf. Rec. IEEE-IAS Annu. Meeting*, New Orleans, Louisiana, Sept. 2007, pp. 1200–1206.

[14] M. Saejia and S. Sangwongwanich, "Averaging analysis approach for stability analysis of speed-sensorless induction motor drives with stator resistance estimation," *IEEE Trans. Ind. Electron.*, vol. 53, no. 1, pp. 162–177, Feb. 2006.

[15] K. Bradley, W. Cao, J. Clare, and P. Wheeler, "Predicting inverter-induced harmonic loss by improved harmonic injection," *IEEE Trans. Power Electron.*, vol. 23, no. 5, pp. 2619–2624, Sept. 2008.

[16] M. Akbaba, M. Taleb, and A. Rumeli, "Improved estimation of induction motor parameters," *Electric Power Systems Research*, vol. 34, no. 1, pp. 65–73, July 1995.

[17] G. R. Slemon, "Modelling of induction machines for electric drives," *IEEE Trans. Ind. Appl.*, vol. 25, no. 6, pp. 1126–1131, Nov./Dec. 1989.

[18] L. O. Chua, "Dynamic nonlinear networks: State-of-the-art," *IEEE Trans. Circuits Syst.*, vol. CAS-27, no. 11, pp. 1059–1087, Nov. 1980.

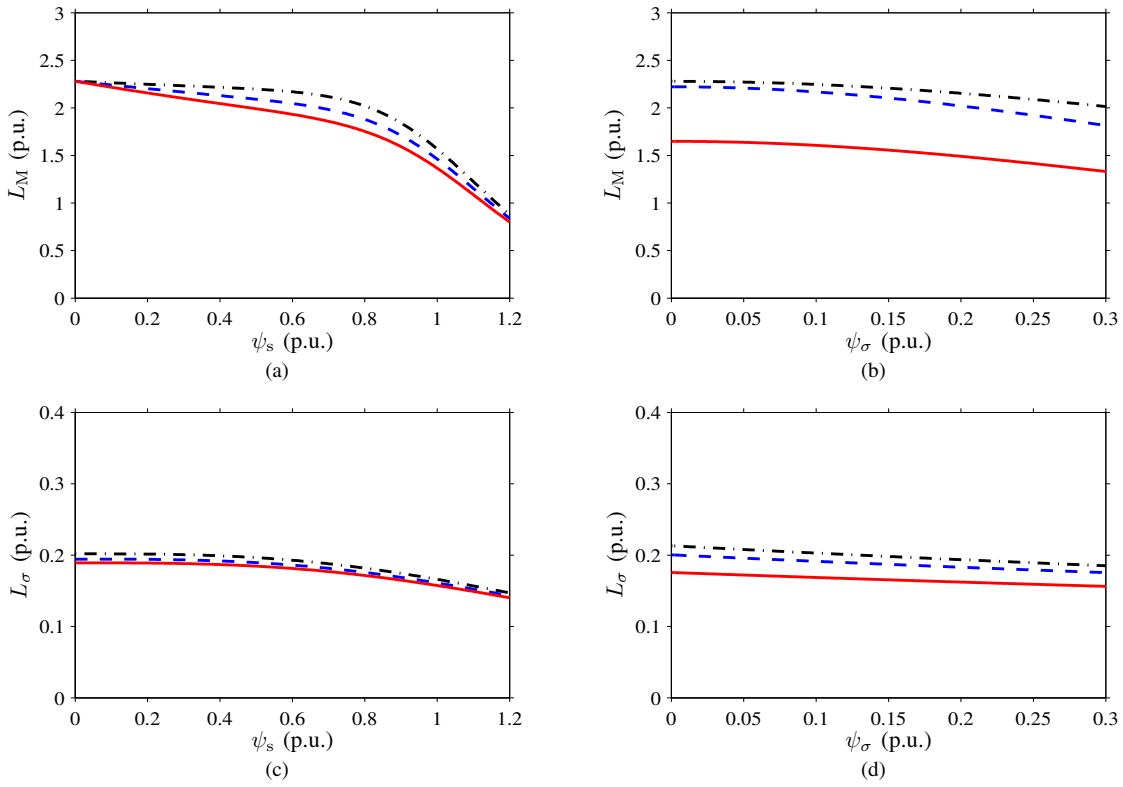

Fig. 9. Results of indirect method applied to experimental data: (a) L_M as a function of ψ_s for three different values of ψ_σ, (b) L_M as a function of ψ_σ for three different values of ψ_s, (c) L_σ as a function of ψ_s for three different values of ψ_σ, (d) L_σ as a function of ψ_σ for three different values of ψ_s. In (a) and (c), the values of ψ_σ are 0.14 p.u. (dash-dotted line), 0.22 p.u. (dashed line) and 0.28 p.u. (solid line). In (b) and (d), the values of ψ_s are 0.4 p.u. (dash-dotted line), 0.7 p.u. (dashed line) and 1.0 p.u. (solid line).

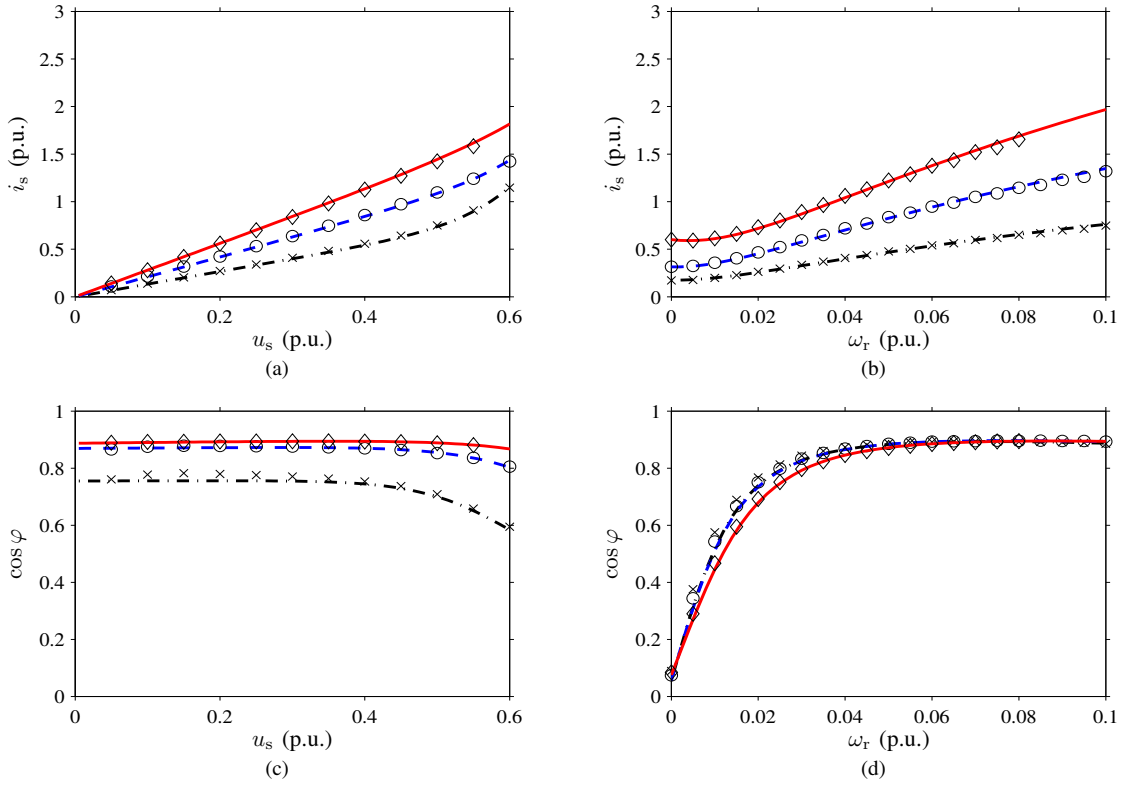

Fig. 10. Results of indirect method applied to experimental data: (a) magnitude of stator current i_s as a function of u_s for three different values of ω_r, (b) i_s as a function of ω_r for three different values of u_s, (c) displacement power factor $\cos\varphi$ as a function of u_s for three different values of ω_r, (d) $\cos\varphi$ as a function of ω_r for three different values of u_s. In (a) and (c), the values of ω_r are 0.0214 p.u. (dash-dotted line), 0.0427 p.u. (dashed line) and 0.0640 p.u. (solid line). In (b) and (d), the values of u_s are 0.2 p.u. (dash-dotted line), 0.35 p.u. (dashed line) and 0.5 p.u. (solid line).

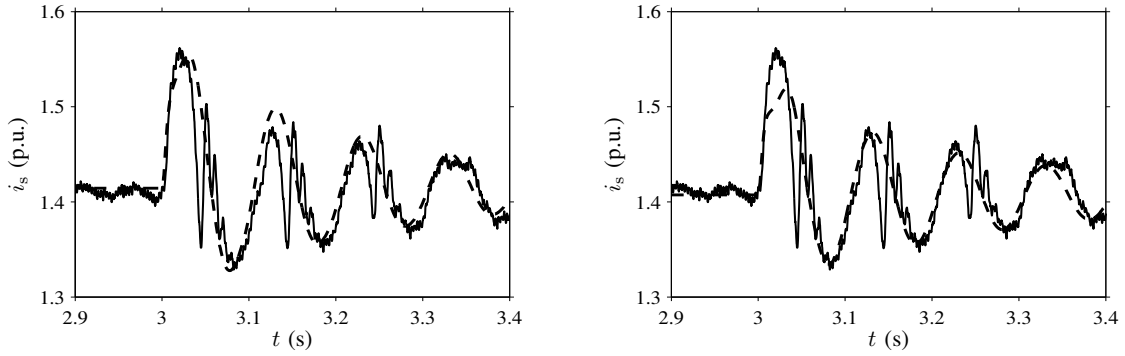

Fig. 11. Experimental and simulation results of the transient test, the magnitude of the stator current vector i_s as a function of time: (a) the simulation model includes the mutual saturation effect, (b) the mutual saturation effect has been omitted. The initial value of ω_s is 0.2 p.u. At t = 3.0 s, ω_s is reversed to -0.2 p.u. The magnitude of the stator voltage is 0.15 p.u. Solid line is the measured stator current, dashed line is the simulated stator current.

[19] S. Shinnaka, "Proposition of new mathematical models with core loss factor for controlling ac motors," in *Proc. IEEE IECON'98*, vol. 1, Aachen, Germany, Aug./Sept. 1998, pp. 297–302.

[20] E. Levi, A. Lamine, and A. Cavagnino, "Impact of stray load losses on vector control accuracy in current-fed induction motor drives," *IEEE Trans. Energy Convers.*, vol. 21, no. 2, pp. 442–450, June 2006.

[21] T. S. Birch and O. I. Butler, "Permeance of closed-slot bridges and its effect on induction motor current computation," *Proc. IEE*, vol. 118, no. 1, pp. 169–172, Jan. 1971.

[22] S. Williamson and M. C. Begg, "Calculation of the bar resistance and leakage reactance of cage rotors with closed slots," *IEE Proc. B, Electr. Power Appl.*, vol. 132, no. 3, pp. 125–132, May 1985.

[23] O. I. Butler and T. S. Birch, "Comparison of alternative skew-effect parameters of cage induction motors," *Proc. IEE*, vol. 118, no. 7, pp. 879–883, July 1971.

[24] K. J. Binns, R. Hindmarsh, and B. P. Short, "Effect of skewing slots on flux distribution in induction machines," *Proc. IEE*, vol. 118, no. 3/4, pp. 543–549, Mar./Apr. 1971.

[25] A. Vagati, M. Pastorelli, F. Scapino, and G. Franceschini, "Impact of cross saturation in synchronous reluctance motors of the trasverse-laminated type," *IEEE Trans. Ind. Appl.*, vol. 36, no. 4, pp. 1039–1046, Jul./Aug. 2000.

[26] J. Luomi, A. Niemenmaa, and A. Arkkio, "On the use of effective reluctivities in magnetic field analysis of induction motors fed from a sinusoidal voltage source," in *Proc. ICEM'86*, vol. 3, Munich, Germany, Sept. 1986, pp. 706–709.

[27] A. Arkkio, "Analysis of induction motors based on the numerical solution of the magnetic field and circuit equations," Doctoral thesis, Dept. Elect. Commun. Eng., Helsinki Univ. Tech., Espoo, Finland, Dec. 1987.

[28] J. K. Pedersen, F. Blaabjerg, J. W. Jensen, and P. Thogersen, "An ideal PWM-VSI inverter with feedforward and feedback compensation," in *Proc. EPE'93*, vol. 4, Brighton, U.K., Sept. 1993, pp. 312–318.